Experiments on the low-Reynolds-number settling of a sphere through a fluid interface

Paul A. Jarvis,[1,2,3,*] Heidy M. Mader,[1] Herbert E. Huppert,[1,2,4] Katharine V. Cashman,[1] and Jon D. Blundy[1]

[1]*School of Earth Sciences, University of Bristol, Bristol, BS8 1RJ, United Kingdom*

[2]*Department of Applied Mathematics and Theoretical Physics, University of Cambridge, Cambridge, CB3 0WA, United Kingdom*

[3]*Department of Earth Sciences, University of Geneva, Geneva, 1205, Switzerland*

[4]*School of Mathematics and Statistics, University of New South Wales, Kensington, Sydney, NSW 2052, Australia*

(Received 26 January 2017; published 20 February 2019)

The low-Reynolds-number gravitational settling of a sphere through a fluid interface is investigated experimentally. By varying the viscosity ratio between the two fluids and the Bond number, two different modes of interfacial deformation are observed: a tailing mode and a film drainage mode. In the tailing mode, the interface deforms significantly as the sphere approaches, and the sphere becomes enveloped by a layer of the upper fluid. A tail forms, connecting the sphere to the bulk of the upper phase. In the film drainage mode, the interface deforms much less and the sphere impacts onto the interface, which either ruptures to form a contact line on the sphere or leaves a very thin wetting film. Additionally, two types of sinking profiles are observed: steady sinking, where the sphere velocity changes monotonically as it sinks, and stalled sinking, where the sphere's progress is inhibited by the interface, before it accelerates into the lower fluid. We present a regime diagram showing the different behaviors. Finally, the dependence of the sinking time on the Bond number and viscosity ratio is investigated. For the film drainage regime a simple scaling law is deduced; the tailing regime exhibits more complicated dynamics, possibly explained by a multistage sinking process.

DOI: 10.1103/PhysRevFluids.4.024003

I. INTRODUCTION

Interactions between particles and fluid interfaces have significant applications in industry and nature. Industrial applications include particle coating [1,2] and separation [3] and the measurement of ultra-low interfacial tensions (IFTs) [4]. Water-walking arthropods supported on a lake surface by surface tension are a common natural example [5,6], while various particle-interface interactions also occur in magmas, which are a mixture of molten liquid (melt), bubbles, and solid crystals. For example, wetting of crystals by bubbles can drive mineral flotation, modifying the spatial distribution of chemical components throughout the magmatic system [7]. Another process is the mixing of magmas of different compositions, commonly invoked as a trigger in volcanic eruption models [8], and the contribution of crystals to the mixing process [9]. A final magmatic example is provided by cored volcanic bombs, fragments of country rock entrained into a magma and then ejected surrounded by a layer of melt [10].

*paul.jarvis@unige.ch

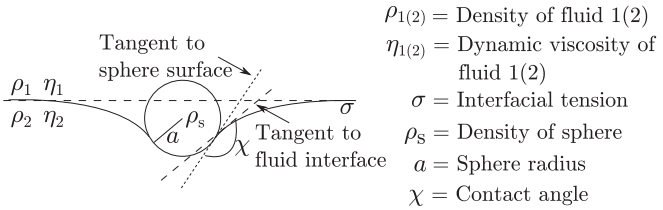

FIG. 1. Sketch of the physical parameters in the system. The sphere is denser than both fluids, i.e., $\rho_s > \rho_2 > \rho_1$. If a three phase contact line exists on the surface of the sphere, the contact angle is defined as χ.

Many of these examples involve small particles and viscous fluids. However, while much research has gone into studying both the conditions at which an interface can support a particle [11–20] and the dynamics of inertial impacts [21–27], there has been relatively little study of the low-Reynolds-number impact of particles onto fluid interfaces [12,28–31]. In particular, questions remain regarding the relative effects of viscous, buoyancy (gravity), and IFT forces on the sinking dynamics. Here we present experimental observations of low-Reynolds-number settling through an interface, along with measurements of the timescale of sinking.

The rest of this introduction defines the problem (Sec. I A), describes prior research (Sec. I B) and presents the questions of the study (Sec. I C). We then describe the experiments (Sec. II) and present and discuss the results (Sec. III) before ending with our conclusions (Sec. IV).

A. Problem description

We are interested in the low-Reynolds-number ($\mathrm{Re} = \rho L U/\eta \ll 1$, where ρ, L, U, and η are characteristic values of the density, length scale, velocity, and dynamic viscosity, respectively) gravitational settling of a sphere through the interface between two density-stratified, immiscible fluids. The parameters of the system are defined in Fig. 1. Dimensional analysis shows that three dimensionless numbers characterize the system: the Bond number Bo, a modified density ratio (MDR) D, and the viscosity ratio λ defined by

$$\mathrm{Bo} = \frac{(\rho_2 - \rho_1) g a^2}{\sigma}, \quad D = \frac{\rho_s - \rho_1}{\rho_2 - \rho_1}, \quad \lambda = \frac{\eta_2}{\eta_1}. \tag{1}$$

Another parameter commonly used in descriptions of interfacial phenomena is the capillary number $\mathrm{Ca} = \eta U/\sigma$. If one defines U to be the terminal velocity in the upper fluid, and $\eta = \eta_1$, then $\mathrm{Ca} = D\mathrm{Bo}$. Hence, the capillary number is not required to form a complete description of the system.

The interface has an intrinsic length scale called the capillary length

$$l_c = \sqrt{\frac{\sigma}{(\rho_2 - \rho_1) g}}. \tag{2}$$

On length scales smaller than l_c, IFT controls the response of the interface to a disturbance, whereas on length scales larger than l_c, the response is controlled by the density contrast between the fluids. Comparing Eqs. (1) and (2), we find that $\mathrm{Bo} = 1$ when $a = l_c$, suggesting a transition in behavior may be seen near $\mathrm{Bo} = 1$.

If the sphere surface and fluid interface meet at a three-phase contact line, one also needs to define the contact angle χ (angle between the tangents to the sphere and fluid surface at the contact) [32]. During the sinking process, the contact line will move and the contact angle will change [33]. In this study, we neglect the dynamics of the moving contact line although they would need to be considered by a more accurate theoretical or numerical study.

To determine the relationships between timescales in the problem and the dimensionless parameters, we nondimensionalize time with respect to a chosen timescale. The large number of

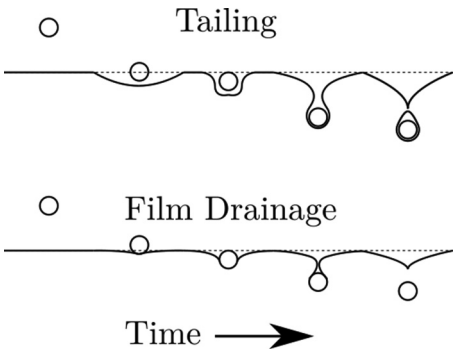

FIG. 2. Sketch showing modes of interfacial deformation. The upper is a tailing mode, the lower, film drainage. The tailing mode leads to significant entrainment of the upper phase into the lower layer.

parameters in the system means there are different choices. One possibility is the Stokes timescale of the upper fluid, t_u [34], defined as the time taken for the sphere to settle a distance of one radius in an infinite volume of the upper fluid. Alternatively, one could also choose the Stokes timescale of the lower fluid t_l. There also exist timescales associated with the IFT, termed capillary timescales of the upper and lower fluid

$$t_{cu} = \frac{\eta_1 a}{\sigma}, \tag{3}$$

and

$$t_{cl} = \frac{\eta_2 a}{\sigma}. \tag{4}$$

In this study, we use the capillary timescale of the upper fluid t_{cu}, although previous studies have employed both t_u [34] and t_{cl} [35]. The different timescales are related to each other through the dimensionless parameters

$$t_{cu} = \frac{2D\mathrm{Bo}\, t_u}{9} = \frac{t_{cl}}{\lambda} = \frac{2(D-1)\mathrm{Bo}\, t_l}{9\lambda}. \tag{5}$$

B. Previous studies

A particle at an interface between two fluids is acted on by gravity, buoyancy, viscous drag, and IFT forces. Much of the prior theoretical work on the interaction between particles and horizontal interfaces has addressed the conditions for which a particle placed instantaneously at the interface can be supported [11–20,36]. Vella [37] provides a review of the conditions required for floating or sinking of particles at an interface, including the effects of geometry, wettability, particle flexibility, and the presence of multiple particles.

These theoretical studies all assume the initial existence of a three-phase contact line on the surface of the particle. The initial condition in our investigation, however, is a sphere moving under gravity towards a fluid interface. It has been shown analytically that the sphere slows down on approach to the interface, according to a factor depending on the sphere-interface separation [38] and the viscosity ratio between the two fluids [28]. However, these models neglect interfacial deformation, and experiments performed to test the models show that spheres settle towards an interface slightly faster than predicted [28].

For a sphere settling onto an interface, two different modes of interfacial deformation have been observed in experiments [39] and numerical models [30]: a film drainage and a tailing mode (Fig. 2). The film drainage mode is characterized by only a small amount of interfacial deformation, and a thin film is created between the sphere and the interface [40]. Theoretical [41,42] and numerical

[43,44] models of film drainage make predictions of the film thickness and drainage rate which agree with experimental observations, although it is difficult to numerically resolve film dynamics for very thin films [44]. While these models do not include film rupture, it has been shown that the film is thinnest at a point off-axis, suggesting the most likely location for rupture [45]. Film rupture, however, requires the formation of a three phase contact line [46] which remains poorly understood. Such contact lines are associated with a line tension [47], but estimates of its size vary over many orders of magnitude [48]. Therefore, we do not discuss this further. Where a three-phase contact line initially exists, Lee and Kim [35] proposed a model describing the low-Reynolds-number sinking of a sphere through an air-liquid interface and derived a scaling relationship for the sinking time depending on the MDR, Bond number, and contact angle (assumed static).

In the tailing mode, the interfacial deformation is significant. Here the interface deforms as the sphere approaches and the sphere is enveloped by the interface. This envelope forms a tail behind the sphere, connecting it to the upper body of fluid. The tail thins as the buoyant fluid drains upward and eventually breaks. Tails have been observed experimentally for a sphere settling into a lower viscosity medium [9,12,34] although the effect of λ on the sinking process to our knowledge has not been considered. Tails have also been observed for the passage of deformable bubbles through fluid interfaces [31,44].

The settling of spheres through interfaces has also been considered numerically using a boundary integral method (BIM). First done for small interfacial deformations [29] and later extended [30], the models reproduce observations of film thinning and tailing mode sinking. However, these models terminate before interface rupture, as the BIM is unable to model topological changes to the interface.

Very recently, Pierson and Magnaudet [26,27] have produced a comprehensive experimental and numerical study of spheres settling through fluid interfaces. The majority of their experiments were performed in inertia-controlled conditions, where they observed three distinct regimes in addition to the flotation, film-drainage, and tailing already mentioned here: three-dimensional tailing, where the axisymmetry is broken; tailing with peripheral corollas (skirt-like instabilities); and tail fragmentation, where the corollas are significant enough to disrupt the tail. These additional regimes occur only when inertia is important, and as such have not been observed in the present study.

All of the above works considered isolated particles. However, some studies have also considered the settling of multiple particles through fluid interfaces, finding that as settling particles slow down at the interface, they can cluster [49]. For the case of particles that can be individually supported at an interface, such clusters form rafts which sink at some critical size [50].

C. Questions

Most of the previous studies on the settling of spheres through fluid interfaces consider intermediate- to high-Reynolds-numbers [1,12,26,34] where inertia is important, meaning there remain a number of unresolved questions in the low-Reynolds-number regime. This investigation seeks to provide a more complete description of such processes, with particular focus on three key issues. First, for what parameter values is a tailing mode observed as opposed to a film drainage configuration? Although observations have been made of both behaviors [12,34,39], quantitative determination of the conditions that control the mode of deformation is incomplete. In particular, the effect of viscosity ratio has been largely ignored. Second, for what conditions is the settling of the sphere inhibited by the interface, i.e., when does the velocity of the sphere as a function of time have a minimum as opposed to monotonically transitioning to the terminal velocity in the lower fluid? To the authors' knowledge, this has not previously been addressed. Finally, how does the sinking time depend on the parameters of the system? Pitois *et al.* [34] found that for very small viscosity ratios ($\lambda \ll 1$), spheres sinking through the tailing mode have a sinking timescale $t_s/t_u \sim 1/\ln(D\mathrm{Bo})$, where t_s is the time between the sphere first touching the plane of the undeformed interface and the moment at which the tail snaps. However, this relationship is based on only five data points and

no fitting is performed. Nor is there any theoretical basis for such a relationship, and variations in the viscosity ratio were not considered. Lee and Kim [35] used an analytical approach to study the sinking of a sphere that was initially stationary at an air-water interface. The mode of sinking was similar to the film drainage mode described above. They proposed a relationship for the sinking time including a term to account for the contact angle

$$\frac{t_s}{t_{cl}} \sim \left[\frac{2D\mathrm{Bo}}{9} - \frac{1}{3}\sin^2\left(\frac{\chi}{2}\right)\right]^{-1}, \tag{6}$$

This model assumes that the flow field in the fluid was the same as for a completely immersed sphere. Comparison with experiments shows the model works well until the point of interface rupture when the sphere loses contact with the bulk of the air. However, this assumption is almost certainly not valid for the case of an interface between two viscous fluids with a viscosity contrast. In this project, the studies of Pitois *et al.* [34] and Lee and Kim [35] are extended to quantify the dependence of sinking time on the viscosity ratio as well as the Bond number, and to consider whether the dominant control on sinking is the IFT or the viscosity contrast.

II. METHODOLOGY

A density-stratified, two-layer fluid system was created in a rectangular cuboid tank (Fig. 3). The lower fluid was a mixture of Tate and Lyle's golden syrup and water, and the upper fluid was a polydimethylsiloxane (PDMS) oil. Spherical ballotini were dropped through a central funnel and allowed to settle through the center of the tank (ensuring consistent wall effects) onto the interface. Filming the experiments allowed the position of the spheres to be tracked and the sinking time and mode of deformation to be determined. The sinking time is defined as the time between the sphere first touching the plane of the undeformed interface and the moment at which it lost contact with the bulk of the upper phase. Details of the measurements of sphere radius and density, and fluid viscosity, density,and IFT are given in the Supplemental Material [51] along with values of the dimensional (Table 1) and dimensionless (Table 2) variables in each experiment.

III. RESULTS AND DISCUSSION

A. Floating or sinking

Figure 4 shows that in the parameter space defined by D and Bo, the experiments separate into a floating and a sinking regime independent of viscosity ratio. These are compared to theoretical regime boundaries calculated from the model of Vella *et al.* [16] for different contact angles. Their model is derived for the case of a sphere placed instantaneously at rest at the interface. However, the results compare favorably if $\chi \gtrsim 3\pi/5 \approx 1.88$ rad (the sphere is preferentially wetted by the upper fluid).

In our study, accurate determination of the contact angle [54] was difficult due to the high fluid viscosities and small sphere radius, although estimates of the contact angle could be made from images of spheres sinking in the film drainage regime. Using two or three frames each from 36 experiments, a mean value of (2.8 ± 0.2) radians was obtained. The spread in the data is due to measurement uncertainty from image resolution and optical distortion by the curved interface. Despite this, it is obvious that the sphere is preferentially wetted by the upper PDMS oil, and the estimated contact angle is consistent with the observed floating-sinking transition. This suggests that the regime boundary is less sensitive to the impact velocity of the sphere and the viscosity ratio than the contact angle, contrasting with the inertial regime where it has been shown that impact can induce sinking [23,26,55].

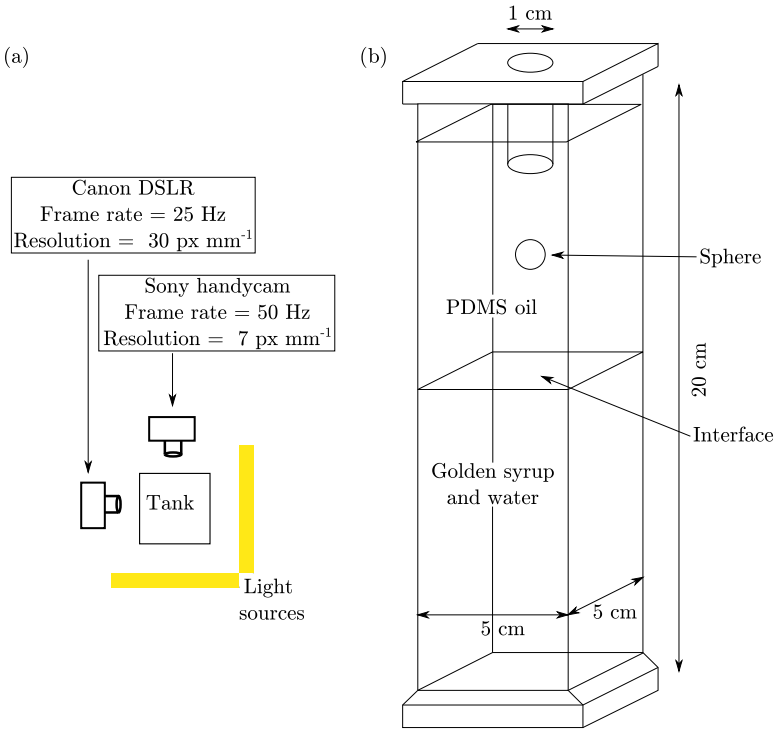

FIG. 3. (a) Aerial view of the experimental setup. The Image-J plug-in MtrackJ [52,53] was used to track the sphere position in the images from the Sony Handycam. Higher resolution images from the Canon DSLR were used to determine both the mode of sinking and the sinking time. In some experiments, the sphere velocity was small enough that the whole tank could be viewed at the slower frame rate of the DSLR, allowing all measurements to be determined from a single set of images. (b) Sketch of the tank used in the experiments. By varying the water content of the syrup solution (0%–5%), the grade of PDMS and the temperature (0–32°), the viscosity ratio was varied between 10^{-2} and 10^{3}. By using spheres from 2 to 10 mm in diameter the Bond number varied from 0.1 to 5.

B. Mode of deformation: Film drainage or tailing

Two modes of deformation are observed: film drainage and tailing [30] (Fig. 5). In both cases, as the sphere approaches the interface, a film of upper-phase fluid fills the gap between sphere and interface. In the film drainage regime [Fig. 5(a)], this film drains just as quickly as the sphere settles, so the interface remains relatively flat as the sphere approaches. The film gradually thins until it either ruptures on the sphere surface or forms a wetting film, too small to be observed. The sphere then slowly sinks through the interface, remaining connected to the interface through a structure similar to a liquid bridge [56], which thins and eventually snaps.

Conversely, in the tailing regime [Fig. 5(b)], the sphere settles towards the interface faster than the film drains upwards, meaning that the interface is substantially depressed by the approach of the sphere. As the sphere passes the original plane of the interface, it becomes enveloped by the film which forms a trailing tail behind the sphere, connecting it to the upper body of fluid. The tail can grow to many sphere radii in length [Fig. 5(c)]. As it extends, it thins and snaps. For tails greater than a few radii in length, the pinching and snapping process propagates down the column, leaving a trail of droplets. This process continues after the sphere has impacted the base of the tank, until only a small volume of upper phase fluid remains attached to the sphere. These tails are very similar to those previously observed for both settling spheres [12,26,34] and rising bubbles [31].

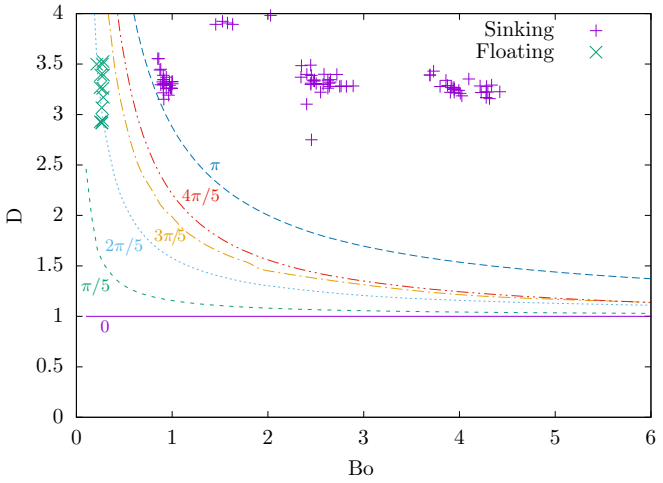

FIG. 4. Regime diagram for floating-sinking. Points show our experimental data. There is a clear divide between floating and sinking, although we have not attempted to constrain the boundary. Curves are calculated from the numerical model of Vella *et al.* [16], see Eqs. (7)–(9) therein, which predicts the transition for a sphere instantaneously placed at the interface, for different values of the contact angle χ. The experiments compare favourably with this model if $\chi \gtrsim 3\pi/5$.

In all but one experiment, the position of snapping is just beneath the plane of the undeformed interface, similar to the "shallow seal" configurations observed for inertial impacts of spheres onto air-water [24] and fluid-fluid [26] interfaces. The exception is experiment G31 ($\mathrm{Bo} = 0.81, D = 3.44, \lambda = 0.018$) where the rupture occurs closer to the sphere. This largely agrees with the results of Pierson and Magnaudet [26], who observed the shallow seal configuration for $\lambda > 0.1$, $\mathrm{Bo} \lesssim$, and $D \lesssim 10$. Pierson and Magnaudet [26] also developed a scaling argument to partially explain the snapping position, but their arguments are valid only for $\mathrm{Re} > 1$, and the presence of viscous dissipation makes it difficult to extend their analysis to the low-Reynolds-number regime.

C. Sinking curve shape

The position curves (height of the sphere with time) define two different types of trajectories (Fig. 6). The first records steady sinking [Fig. 6(a)], where the sphere slows as it approaches the interface and continues to slow as it passes through. The decrease in velocity is monotonic until a new terminal velocity is reached. The second mode describes stalled sinking [Fig. 6(b)], where the sphere slows as it approaches the interface but then accelerates to a new terminal velocity in the lower fluid. In no experiments was a sudden change in fall velocity observed at the moment the interface snapped. We interpret that for steady sinking, the viscosity contrast is the dominant control on the position curve shape, whereas the IFT is the dominant control for stalled sinking.

D. Regime diagram

Figure 7 is a regime diagram in the space defined by Bo and λ for both the mode of deformation (film drainage or tailing) and the shape of the position curve (steady or stalled sinking). An experiment is considered to be in the tailing regime if a continuous film of the upper fluid surrounds the sphere once it has settled through the initial plane of the interface. Detection of the fluid film depends on the optical resolution of the image, which is typically 22 pixels (px) mm^{-1}. Films with a thickness of about 5 px can be distinguished; thus in all tailing experiments reported here the sphere is surrounded by a film at least 0.23 mm thick. For a given Bond number, the film drainage regime

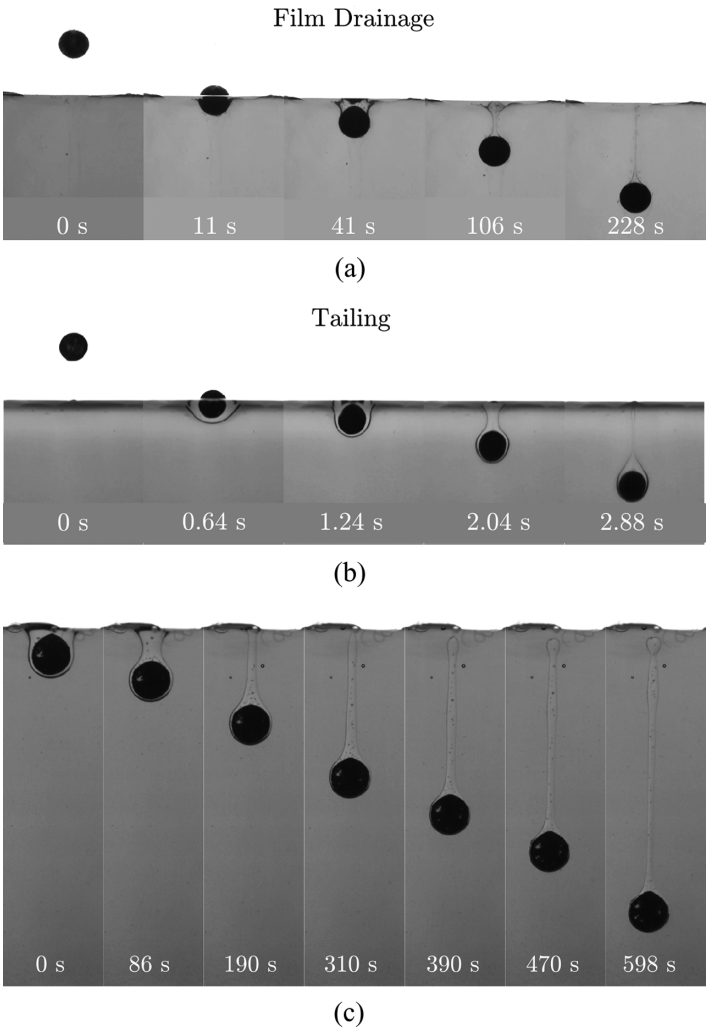

FIG. 5. Images of modes of deformation. (a) Film drainage (Bo $= 4.0$, $D = 3.2$, $\lambda = 260$; experiment F42 in the Supplemental Material [51]). (b) Tailing (Bo $= 2.4$, $D = 3.5$, $\lambda = 4.0$; experiment D24). (c) Tailing with a long tail (Bo $= 4.3$, $D = 3.2$, $\lambda = 1.7$; experiment I14). Videos of these experiments can be found in the Supplemental Material [51].

always occurs at higher viscosity ratios than the tailing regime. For Bo ≈ 4, the transition from tailing to film drainage (purple curve) occurs at $\lambda \approx 30$, and as Bo decreases, the transition moves to smaller values of λ; for example, at Bo $= 1$ it occurs at $\lambda \approx 15$. For smaller viscosity ratios, the transition occurs at Bond numbers smaller than have been investigated. For some experiments, the optical resolution of the images made it difficult to determine the mode of deformation; these have been labeled as transitional. Experiments where floating was observed have been plotted, and we observed no effect of the viscosity ratio on the floating-sinking transition. These can be considered an extreme case of stalled sinking, where the IFT is strong enough to support the sphere at the interface indefinitely despite the density contrast.

These observations can be understood by considering the effect of Bo and λ on the rate of drainage of the upper phase film between the sphere and the interface relative to the settling velocity. As λ decreases (η_1 increases relative to η_2), the strain rate induced in the lower fluid increases

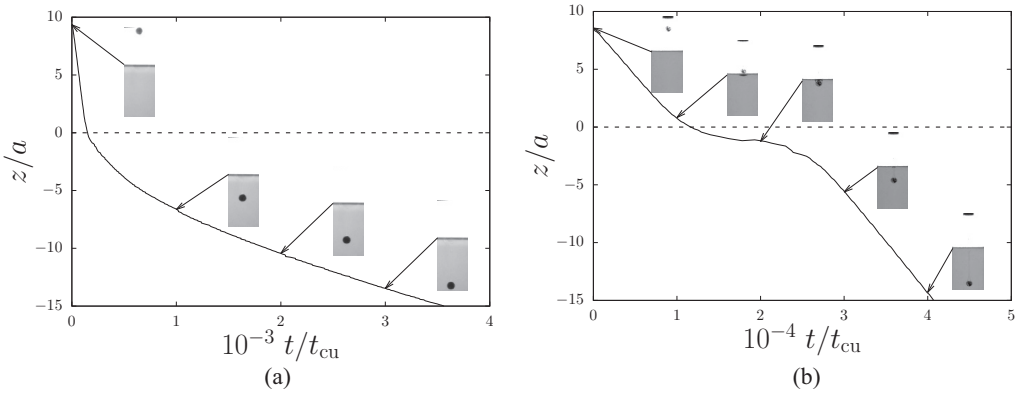

FIG. 6. Two different shapes of position curve seen in experiments. The dashed line shows the initial interface position. Both cases show a transition from the terminal velocity in the upper fluid to a new terminal velocity in the lower fluid. (a) Steady sinking (Bo $= 3.6$, $D = 3.38$, $\lambda = 35$; experiment D15 in the Supplemental Material [51]). The sphere slows on approach to the interface and steadily decelerates to a new slower velocity. (b) Stalled sinking (Bo $= 2.5$, $D = 3.31$, $\lambda = 0.45$; experiment G15). The sphere slows while approaching the interface and appears to stall there before accelerating to a new terminal velocity as it moves away. In both cases the greatest deceleration occurs just below $z = 0$.

relative to that in the film. The net effect is that the sphere settles faster than the film can drain upwards, leading to interface deformation and the formation of a tail. Alternatively, increasing λ increases the relative strain rate in the film, which drains before the sphere can settle into the lower phase (film drainage mode). Decreasing Bo increases the stress discontinuity that can be maintained at the interface, leading to a smaller stress transmitted to the lower phase, which in turn induces a

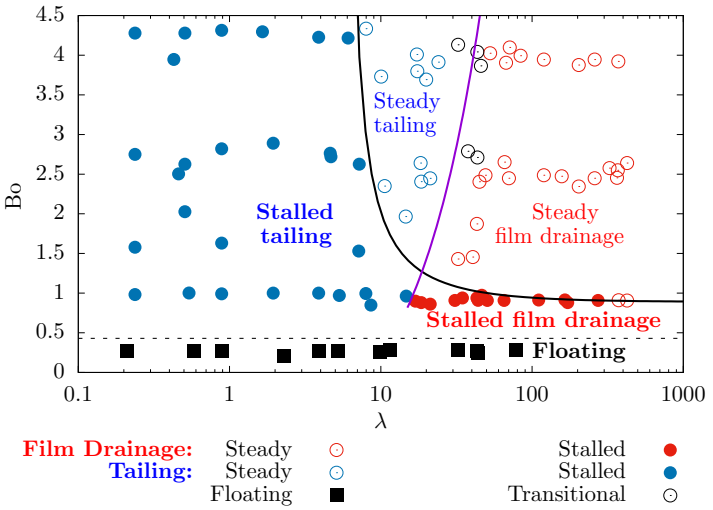

FIG. 7. Regime diagram for both mode of deformation (Fig. 5) and position curve shape (Fig. 6). Distinct regimes can be seen for film drainage (red) and tailing (blue). Points labeled transitional correspond to experiments where the optical resolution of the image meant it was difficult to identify the mode of deformation. The purple line is drawn to help visibly separate the regimes. The different shapes of position curve, steady (hollow symbols) and stalled (solid symbols) sinking, also separate into distinct regimes, with the black curve a fitted theoretical relationship for the transition [Eq. (13)].

smaller strain rate in the lower fluid, and therefore less deformation of the interface. Theoretical prediction of these timescales requires a sophisticated model accounting for coupling between the motions of the sphere and the interface. The curvature of the interface and the discontinuity in fluid properties across it makes this a nontrivial problem necessitating a numerical solution, going beyond the scope of this work.

For a fixed Bond number an increase in the viscosity ratio causes the position curve to transition from stalled to steady sinking (black curve). For Bo > 1 this transition occurs at $5 < \lambda < 10$; for smaller Bond numbers the transition moves to higher viscosity ratios and reaches $\lambda \approx 400$ for Bo $\approx$ 1. This behavior can be simply explained. First, consider the scenario of zero IFT (Bo $\to \infty$). In this case, the sinking profile must be steady if the terminal velocity in the lower layer is less than that in the upper layer ($u_{t,2} < u_{t,1}$). In dimensionless parameters, this is realized when

$$\lambda > 1 - \frac{1}{D}. \tag{7}$$

In our experiments $D \approx 3.5$, so this condition corresponds to $\lambda > 0.7$. However, as Fig. 7 shows, the transition from stalled to steady sinking occurs for λ at least an order of magnitude greater throughout the investigated range of Bo because of the effect of IFT. When the IFT decelerates the sphere to a velocity less than the terminal velocity in the lower layer, stalled sinking is observed. Conversely, when the viscosity ratio is sufficiently large that the increase in viscosity controls the deceleration, then sinking is steady. For Bo ≈ 1, the transition between the two regimes occurs at an order of magnitude larger than for Bo ≈ 1.5. This is because the capillary length is now comparable to the sphere radius, meaning the IFT completely dominates the resistive force slowing the sphere.

We use these results to inform a semi-empirical model describing the stalled-steady sinking transition. The model relies on an assumption that the sphere settles in a quasisteady fashion, such that the forces on the sphere (weight F_w, buoyancy F_b, IFT F_σ, and viscous drag F_η) are in balance at all times t, i.e., $F_w(t) = F_\eta(t) + F_b(t) + F_\sigma(t)$. This is valid for Stokes flow. Then, motivated by the expression for viscous drag on an immersed sphere in a infinite fluid, we express the viscous drag force as $F_\eta = f(t)V(t)$, where $V(t)$ is the settling velocity of the sphere and the function $f(t)$ depends on the viscosities of the two fluids, as well as containing information on the sphere and interface position. One can then write

$$V(t) = \frac{F_w(t) - F_b(t) - F_\sigma(t)}{f(t)}. \tag{8}$$

Initially, $V = u_{t,1}$, and once the sphere has passed the interface, $V(t_{end}) \to u_{t,2}$. Stalled sinking occurs if $V(t)$ has a minimum at some time t. Given the difficulties of determining the functions $F_b(t)$, $F_\sigma(t)$, and $f(t)$, we approximate them by expressions with functional forms motivated by physics but with adjustable fitting parameters. We assume that the buoyancy force can be expressed as a weighted sum of its values when the sphere is fully immersed in the lower and upper fluids

$$F_b(t) = \frac{4\pi a^3 g\{\alpha(t)\rho_1 + [1 - \alpha(t)]\rho_2\}}{3}, \quad \text{where} \quad 0 \leqslant \alpha(t) \leqslant 1. \tag{9}$$

The function $f(t)$ is taken to be a similarly weighted sum

$$f(t) = 6\pi a\{\gamma(t)\eta_1 + [1 - \gamma(t)]\eta_2\}, \quad \text{where} \quad 0 \leqslant \gamma(t) \leqslant 1. \tag{10}$$

We approximate the IFT force to be proportional to the maximum value an interface can exert on a sphere at a fluid interface [16,36]

$$F_\sigma(t) = 2\beta(t)\pi a\sigma, \quad \text{where} \quad 0 \leqslant \beta(t) \leqslant 1. \tag{11}$$

Finally, at all times the weight of the sphere is given by $F_w = 4\pi a^3 \rho_s/3$. Stalled sinking therefore occurs if at some time t, $V(t) < u_{t,2}$. Following algebraic manipulation, this can be shown to be

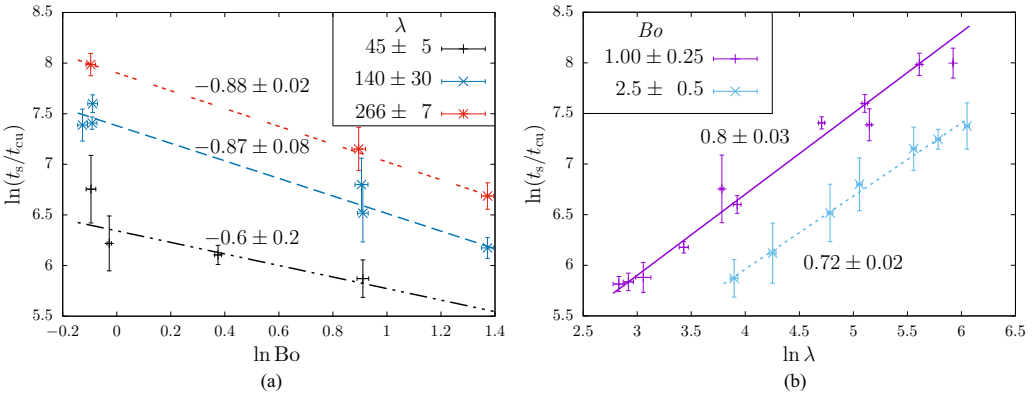

FIG. 8. For the film drainage experiments, the dependence of the dimensionless sinking time on (a) the Bond number and (b) the viscosity ratio. The lines are the result of a linear fit and the gradients are stated.

equivalent to

$$\mathrm{Bo} < \frac{3\beta(t)\lambda}{2\{\gamma(t)(1-D)+\lambda[\alpha(t)-\gamma(t)(1-D)]\}}. \tag{12}$$

Since the functions $\alpha(t)$, $\beta(t)$ and $\gamma(t)$ contain the complexity associated with the evolving shape of the interface and stress discontinuity across it, it is difficult to determine any more about their properties without further sophisticated analysis. Therefore, we define the time $t = T$ as that which maximizes the right-hand side of Eq. (12), and further define $\delta = 2\gamma(T)/[3\beta(T)]$ and $\epsilon = 2\alpha(T)/[3\beta(T)]$. The condition for stalled sinking then becomes

$$\mathrm{Bo} < \frac{\lambda}{\delta(1-D)+\lambda[\epsilon+\delta(1-D)]}. \tag{13}$$

Given the sparsity of constraints on the transition curve (Fig. 7), we do not perform a quantitative fitting, but rather explore the different values of δ and ϵ that produce a curve correctly describing the observed transition. We find that Eq. (13) accurately describes the transition if $\delta = 2.5 \pm 0.4$ and $\epsilon = 5.0 \pm 0.9$.

E. Sinking timescale

We define the sinking time as the time from when the sphere first touches the original plane of the interface to the moment when it loses contact with the bulk of the upper phase (i.e., when the tail or bridge connecting the sphere to the bulk of the upper layer snaps). Tables 3 and 4 in the Supplemental Material [51] show the raw data. The formation of a contact line during the film drainage mode suggests that film drainage and tailing modes have different dynamics. Therefore they are considered separately.

By grouping experiments with similar values of λ and Bo, we see that in the film drainage regime, the dimensionless sinking time decreases with the Bond number [Fig. 8(a)] and increases with the viscosity ratio [Fig. 8(b)]. Neither of these trends are surprising. As the viscosity ratio increases, the strain rate induced in the lower fluid by the sphere decreases, and so the velocity of the displaced fluid decreases (i.e., sinking takes longer). Additionally, as the Bond number increases, the magnitude of gravitational forces increases relative to the IFT forces, leading to more rapid sinking. Both relationships appear to be well fitted by power laws, so we assume that the sinking time can be described by a relationship of the form

$$\frac{t_s}{t_{cu}} \sim \mathrm{Bo}^{\,a}\lambda^{b} \tag{14}$$

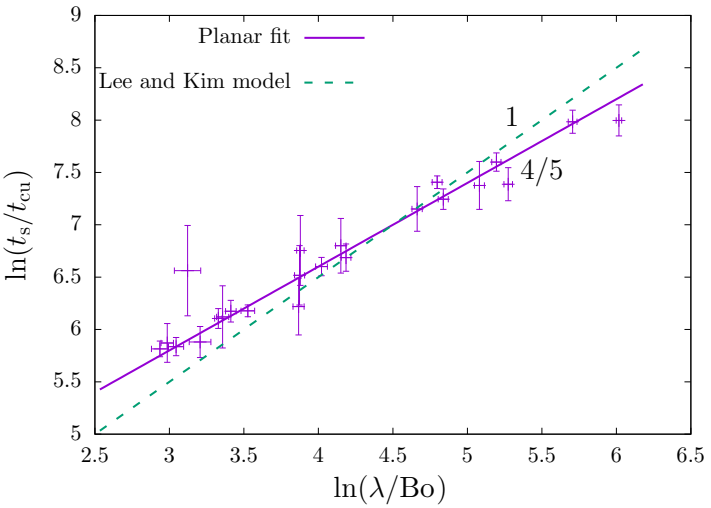

FIG. 9. A log-log plot of the dimensionless sinking time against the viscosity ratio divided by the Bond number. The solid line has a gradient of 4/5, as calculated from the planar fit and does a good job of describing the data. The dashed line has a gradient of 1, as predicted by Lee and Kim [35], and has been positioned to provide the closest fit to our data.

or

$$\ln\left(\frac{t_s}{t_{cu}}\right) \sim a \ln \mathrm{Bo} + b \ln \lambda. \tag{15}$$

A planar fit to all the data yields $a = -0.80 \pm 0.05$ and $b = 0.80 \pm 0.02$ (Fig. 9), which has a chi-squared value of 0.939. This means that the empirical law for the film drainage configuration can be expressed as

$$\frac{t_s}{t_{cu}} \sim \left(\frac{\lambda}{\mathrm{Bo}}\right)^{0.8} = \left(\frac{\lambda}{\mathrm{Bo}}\right)^{4/5}. \tag{16}$$

In their investigation of the low-Reynolds-number sinking of a sphere through an air-liquid interface, Lee and Kim [35] assumed a sinking configuration similar to the film drainage seen here. Their simple scaling analysis assumes a constant sinking velocity and predicts that, for a constant MDR and contact angle, $t_s/t_{cl} \sim (\mathrm{Bo})^{-1}$ [see Eq. (6)], which corresponds to $t_s/t_{cu} \sim (\lambda/\mathrm{Bo})^{-1}$ [35]. This is close to our result, with the discrepancy likely due to the assumption of a constant velocity in the scaling analysis, which while possibly valid for an air-water interface, is certainly not for our experiment.

For the tailing regime, the dependence of the sinking time on Bo and λ is more complicated, with no simple power-law relationship. To simplify the problem we divide the sinking process into three stages (Fig. 10): (a) pushing (timescale t_p), when the sphere traverses the plane of the initial interface; (b) thinning (t_c), when the tail thins until its minimum thickness is equal to the capillary length; and (c) snapping (t_s), when the tail pinches off. Although somewhat arbitrary, these definitions are motivated by the processes that must occur at each stage. The pushing stage requires the displacement of both fluids as the sphere settles. The thinning stage involves the balance between downward entrainment and buoyant rise of the tail fluid. Finally, once the column thickness becomes comparable to l_c, the IFT acts to snap the tail.

Figure 10 shows that t_p/t_{cu} decreases with Bo, with the rate of change greatest close to $\mathrm{Bo} = 1$. This is intuitive since as $\mathrm{Bo} \to 1$, the relative strength of IFT forces increases, thus requiring more kinetic energy from the sphere to deform the interface, which decelerates the sphere and increases

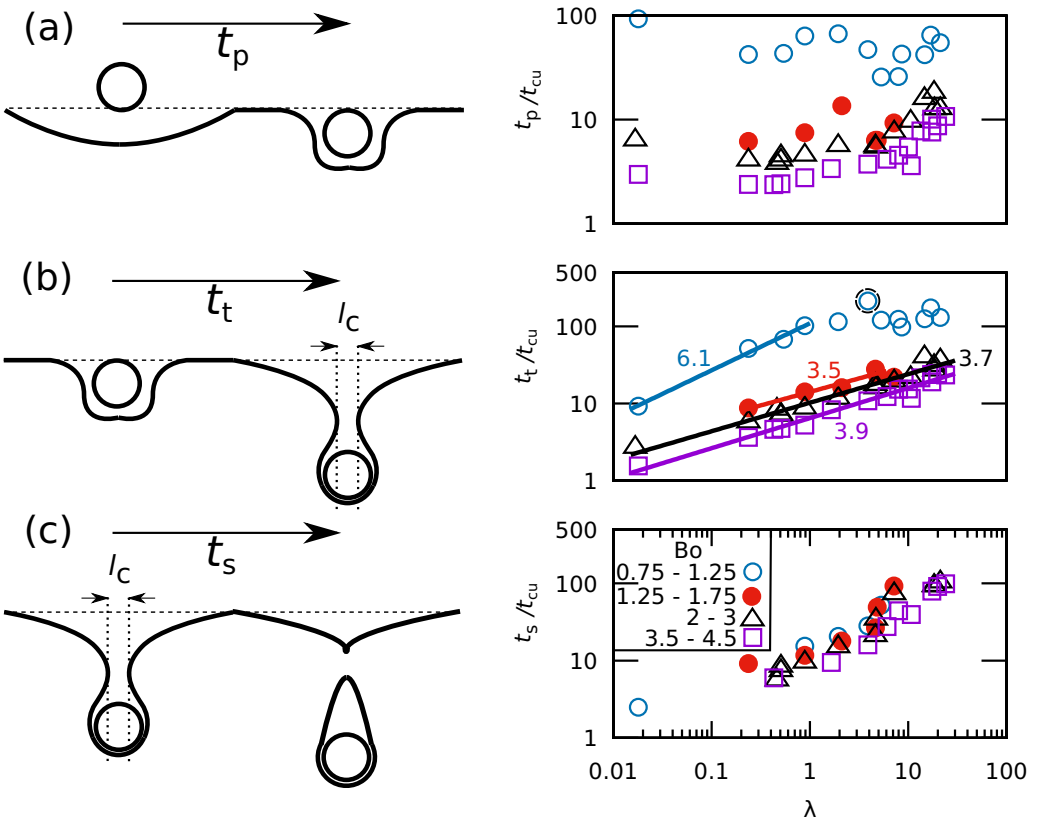

FIG. 10. Tailing mode was divided into three stages: (a) pushing, when the sphere traverses the plane of the initial interface, (b) thinning, when the tail thins until its thickness is equal to the capillary length, and (c) snapping, when the tail pinches off. The dependence of the dimensionless time of each stage on Bo and λ is shown. (a) t_p/t_{cu} decreases with Bo for Bo > 1 and is nonmonotinic with λ. (b) t_t/t_{cu} decreases with Bo and increases with λ. Linear fits are provided for Bo > 1 and Bo $\approx 1, \lambda < 1$. Measurement uncertainty is comparable to the symbol size. One point (circled with a dashed line) has an anomalously high value. c) t_s/t_{cu} depends only weakly on Bo, as can be seen by the collapse of the curves on the plot against λ.

the sinking time. The dependence on λ is nonmonotonic, with each curve displaying at least one minimum. For all values of Bo investigated, there is a minimum at $0.2 < \lambda < 0.5$. This is perhaps surprising, because one might expect the t_p/t_{cu} to decrease continuously as λ decreases, since this corresponds to a reduction in the relative viscosity of the lower fluid. However, decreasing λ also increases the volume of the upper phase film that is entrained during the pushing process. This reduces the net density of the sphere and entrained fluid, which can also increase t_p/t_{cu}. Therefore there is a critical value of λ at which the entrained volume becomes large enough to overcome the decreasing viscous resistance. The curves for Bo ≈ 1, 1.5, and 2.5 also contain a second minimum at $\lambda \approx 5$, which can be explained by the increasing effect of IFT as Bo decreases towards 1. The increase in IFT reduces the volume of entrained fluid, increasing the bulk density of the sphere and the enveloping fluid, which decreases the sinking time.

The behavior of t_t/t_{cu} is simpler and decreases with Bo. As with the pushing stage, a smaller Bo means the IFT is strong enough to support the hydrostatic pressure gradient across the tail interface and so reduces the inward velocity of the surrounding fluid. Additionally, t_t/t_{cu} increases with λ, since increasing in the relative viscosity of the lower fluid slows the sinking of the sphere. For Bo > 1, this can be well described by a power law with exponent 3.7 ± 0.2. For Bo $= 1$, however,

t_t/t_{cu} increases with λ for $\lambda < 1$, although at a faster rate than for Bo > 1. For $\lambda > 1$, there seems to be little dependence on Bo. The different behavior observed for Bo > 1 and Bo $= 1$ can be explained by the equality of the sphere radius and capillary length. This means that the tail thickness is only a little larger than l_c throughout the thinning stage, which increases the significance of IFT forces. Different behaviors for Bo $= 1$ and Bo > 1 can also be seen in measurements of the tail length at the moment of snapping (Supplemental Material [51]).

Finally, Fig. 10(c) shows that the snapping timescale t_s/t_{cu} is only weakly dependent on Bo and negligible for $\lambda \gtrsim 10$. This is because snapping occurs just below the initial plane of the interface and away from the sphere and so is independent of the sphere size.

IV. CONCLUSIONS

The low-Reynolds-number gravitational settling of a sphere onto and through a fluid interface has been investigated experimentally for a range of viscosity ratios and Bond numbers, and observations have been made of the deformational mode of the interface and the time taken for sinking. Viscosity ratios were varied between 10^{-2} and 10^3 and Bond numbers between 1 and 5. Two different modes of interfacial deformation were observed: a tailing mode and a film drainage mode. In the tailing mode the interface is significantly deformed during the approach of the sphere. As the sphere passes through the plane of the undeformed interface, it is enveloped by a layer of the upper phase, which forms a tail behind the sphere connecting it to the bulk of the upper fluid. Eventually this tail becomes unstable and snaps. In the film drainage case, the interface deforms to a much smaller extent, and the sphere impacts the interface to form either a contact line or a very thin wetting film. The sphere then slowly sinks through the interface. For Bo > 1 the transition from tailing to film drainage appears independent of the viscosity ratio and occurs at $\lambda \approx 30$, with the tailing regime occurring for smaller viscosity ratios. For Bo $\lesssim 1$ the viscosity ratio at which the transition occurs shifts to lower values. The regime diagram of Fig. 7 can be useful for choosing suitable fluids for particle coating Tsai *et al.* [2] and informing models describing the roles of crystals in magma mixing [9].

We also investigated how the sinking time scales for the different deformational modes. For the film drainage regime, we find for the first time that the sinking time can be described by the power-law relationship $t_s/t_{cu} \sim (\lambda/\text{Bo})^{4/5}$ (Fig. 9). The relationship is more complicated for the tailing mode since λ and Bo have different effects at different stages of sinking. Generally, decreasing Bo increases the sinking time due to the increasing strength of IFT forces, but increasing λ can either increase or decrease the time required for the sphere to traverse the interface, dependent upon the volume of upper phase fluid entrained with the sphere.

This study has provided new empirical results for the timescale of sinking and a regime diagram for the sinking regime. Simple scalings have been unable to reproduce the observed behavior, suggesting more complete theoretical models are required. Such models will need to account for the effect of entrained upper fluid on the dynamics of the sphere and the time dependence of the buoyancy, viscous and IFT forces as the sphere sinks. Including these features would be challenging in a theoretical model, and full numerical simulation may be required to obtain useful results.

ACKNOWLEDGMENTS

This work was supported by the National Environmental Research Council (grant number NE/K500823/1). The authors thank Jeremy Phillips, Nick Teanby, Alison Rust, and Steve Tait for valuable discussions, and Dominic Vella for his insight and the use of his MATLAB script for the production of Fig. 4. The tank used in the experiments was constructed by Charles Clapham, to whom we are grateful. Interfacial tension measurements were made in the Krüss Surface Science Centre at the School of Chemistry, University of Bristol, and P.A.J thanks Richard Schubert-Rowles for his training and assistance. H.E.H acknowledges the support of a Leverhulme Emeritus Fellowship. K.V.C. acknowledges funding from the AXA Research Fund and a Wolfson

Merit Award from the Royal Society. The authors also thank the editor, Howard Stone, and two anonymous reviewers for their comments, which helped to greatly improve the manuscript.

[1] N. Dietrich, S. Ponchin, and H. Z. Li, Dynamical deformation of a flat liquid-liquid interface, Exp. Fluids **50**, 1293 (2011).
[2] S. S. H. Tsai, J. S. Wexler, J. Wan, and H. A. Stone, Conformal coating of particles in microchannels by magnetic forcing, Appl. Phys. Lett. **99**, 153509 (2011).
[3] J. A. Stoos and L. G. Leal, Particle motion in axisymmetric stagnation flow toward an interface, AIChE J. **35**, 196 (1989).
[4] S. S. H. Tsai, J. S. Wexler, J. Wan, and H. A. Stone, Magnetic ultralow interfacial tensiometry with magnetic particles, Lab Chip **13**, 119 (2013).
[5] J. W. M. Bush and D. L. Hu, Walking on water: Biolocomotion at the interface, Annu. Rev. Fluid Mech. **38**, 339 (2006).
[6] D. L. Hu and J. W. M. Bush, The hydrodynamics of water walking arthropods, J. Fluid Mech. **644**, 5 (2010).
[7] M. Edmonds, Flotation of magmatic minerals, Geology **43**, 655 (2015).
[8] S. R. J. Sparks, H. Sigurdsson, and L. Wilson, Magma mixing: A mechanism for triggering acid explosive eruptions, Nature (London) **267**, 315 (1977).
[9] C. J. Renggli, S. Wiesmaier, C. P. De Campos, K. Hess, and D. B. Dingwell, Magma mixing induced by particle settling, Contrib. Mineral. Petrol. **171**, 96 (2016).
[10] G. Sottili, J. Taddeucci, and D. M. Palladino, Constraints on magma-wall rock thermal interaction during explosive eruptions from textural analysis of cored bombs, J. Volcanol. Geotherm. Res. **192**, 27 (2010).
[11] H. M. Princen and S. G. Mason, Shape of a fluid drop at a fluid-liquid interface. II. Theory for three-phase systems, J. Colloid Sci. **20**, 246 (1965).
[12] H. C. Maru, D. T. Wasan, and R. C. Kintner, Behaviour of a rigid sphere at a liquid-liquid interface, Chem. Eng. Sci. **26**, 1615 (1971).
[13] A. V. Rapacchietta, A. W. Neumann, and S. N. Omenyi, Force and free energy analyses of small particles at fluid interfaces 1. Cylinders, J. Colloid Interf. Sci. **59**, 541 (1977).
[14] A. V. Rapacchietta and A. W. Neumann, Force and free energy analyses of small particles at fluid interfaces. 2. Spheres, J. Colloid Interf. Sci. **59**, 555 (1977).
[15] T. I. Hesla and D. D. Joseph, The maximum contact angle at the rim of a heavy floating disk, J. Colloid Interf. Sci. **279**, 186 (2004).
[16] D. Vella, D. Lee, and H. Kim, The load supported by small floating objects, Langmuir **22**, 5979 (2006).
[17] D. J. R. Vella, The fluid mechanics of floating and sinking, Ph.D. thesis, University of Cambridge 2007.
[18] J. Liu, X. Feng, and G. Wang, Buoyant force and sinking conditions of a hydrophobic thin rod floating on water, Phys. Rev. E **76**, 066103 (2007).
[19] C. W. Extrand and S. I. Moon, Critical meniscus height of liquids at the circular edge of cylindrical rods and disks, Langmuir **25**, 992 (2009).
[20] C. W. Extrand and S. I. Moon, Will it float? Using cylindrical disks and rods to measure and model capillary forces, Langmuir **25**, 2865 (2009).
[21] G. Birkhoff and E. H. Zarantonello, *Jets, Wakes and Cavities* (Cambridge University Press, Cambridge, 1957).
[22] C. Duez, C. Ybert, C. Clanet, and L. Bocquet, Making a splash with water repellency, Nat. Phys. **3**, 180 (2007).
[23] D. Lee and H. Kim, Impact of a superhydrophobic sphere onto water, Langmuir **24**, 142 (2008).
[24] J. M. Aristoff and J. W. M. Bush, Water entry of small hydrophobic spheres, J. Fluid Mech. **619**, 45 (2009).
[25] T. T. Truscott, B. P. Epps, and J. Belden, Water entry of projectiles, Annu. Rev. Fluid Mech. **46**, 355 (2014).

[26] J. Pierson and J. Magnaudet, Interial settling of a sphere through an interface. Part 1. From sphere flotation to wake fragmentation, J. Fluid Mech. **835**, 762 (2018).
[27] J. Pierson and J. Magnaudet, Interial settling of a sphere through an interface. Part 2. Sphere and tail dynamics, J. Fluid Mech. **835**, 808 (2018).
[28] E. Bart, The slow unsteady settling of a fluid sphere toward a flat fluid interface, Chem. Eng. Sci. **23**, 193 (1968).
[29] S. H. Lee and L. G. Leal, The motion of a sphere in the presence of a deformable interface II. A numerical study of the translation of a sphere normal to an interface, J. Colloid Interf. Sci. **87**, 81 (1982).
[30] A. S. Geller, S. H. Lee, and L. G. Leal, The creeping motion of a spherical particle normal to a deformable interface, J. Fluid Mech. **169**, 27 (1985).
[31] M. Manga and H. A. Stone, Low Reynolds number motion of bubbles, drops and rigid spheres through fluid-fluid interfaces, J. Fluid Mech. **287**, 279 (1995).
[32] S. A. Safran, *Statistical Thermodynamics of Surfaces, Interfaces, and Membranes* (Addison-Wesley, New York, 1994).
[33] J. H. Snoeijer and B. Andreotti, Moving contact lines: Scales, regimes, and dynamical transitions, Annu. Rev. Fluid Mech. **45**, 269 (2013).
[34] O. Pitois, P. Moucheront, and C. Weill, Franchissement d'interface et enrobage d'une sphère, C. R. Acad. Sci. Paris **327**, 605 (1999).
[35] D. Lee and H. Kim, Sinking of small sphere at low Reynolds number through interface, Phys. Fluids **23**, 072104 (2011).
[36] J. B. Keller, Surface tension force on a partly submerged body, Phys. Fluids **10**, 3009 (1998).
[37] D. Vella, Floating versus sinking, Annu. Rev. Fluid Mech. **47**, 115 (2015).
[38] H. Brenner, The slow motion of a sphere through a viscous fluid towards a plane surface, Chem. Eng. Sci. **16**, 242 (1961).
[39] J. W de Folter, V. W. A. de Villeneuve, D. G. A. L. Aarts, and H. N. W. Lekkerkerker, Rigid sphere transport through a colloidal gas-liquid interface, New J. Phys. **12**, 023013 (2010).
[40] V. W. A. de Villeneuve, D. G. A. L. Aarts, and H. N. W. Lekkerkerker, Comparing the approach of a rigid sphere and a deformable droplet towards a deformable fluid surface, Colloid. Surf. A **282-283**, 61 (2006).
[41] S. Hartland, The profile of the draining film between a rigid sphere and a deformable fluid-liquid interface, Chem. Eng. Sci. **24**, 987 (1969).
[42] A. F. Jones and S. D. R. Wilson, The film drainage problem in droplet coalescence, J. Fluid Mech. **87**, 263 (1978).
[43] P. G. Smith and T. G. M. Van de Ven, The effect of gravity on the drainage of a thin liquid film between a solid sphere and a liquid/fluid interface, J. Colloid Interf. Sci. **100**, 456 (1984).
[44] R. Bonhomme, J. Magnaudet, F. Duval, and B. Piar, Inertial dynamics of air bubbles crossing a horizontal fluid-fluid interface, J. Fluid Mech. **707**, 405 (2012).
[45] S. Hartland, The approach of a rigid sphere to a deformable liquid/liquid interface, J. Colloid Interf. Sci. **26**, 383 (1968).
[46] A. Schelduko, B. V. Toshev, and D. T. Bojadjiev, Attachment of particles to a liquid surface (capillary theory of flotation), J. Chem. Soc. Faraday T **72**, 2815 (1975).
[47] J. W. Gibbs, *The Scientific Papers of J. Willard Gibbs, Vol. 1* (Ox Bow Press, Connecticut, Woodbridge, 1961).
[48] B. M. Law, S. P. McBride, J. Y. Wang, H. S. Wi, G. Paneru, S. Betelu, B. Ushijima, Y. Takata, B. Flanders, F. Bresme *et al.*, Line tension and its influence on droplets and particles at surfaces, Prog. Surf. Sci. **92**, 1 (2017).
[49] M. Manga, The motion of deformable drops and bubbles at low Reynolds number: Applications to selected problems in geology and geophysics, Ph.D. thesis, Harvard University 1994.
[50] S. G. Jones, N. Abbasi, A. Ahuja, V. Truong, and S. S. H. Tsai, Floating and sinking of self-assembled spheres on liquid-liquid interfaces: Rafts versus stacks, Phys. Fluids **27**, 072102 (2015).
[51] See Supplemental Material at http://link.aps.org/supplemental/10.1103/PhysRevFluids.4.024003 for in-depth description of measurements of fluid and particle properties, tabulated experimental data, results

on the lenght of tails, and movies of the experiments. Captions for the movies can be found in the README.TXT file.

[52] C. A. Schneider, W. S. Rasband, and K. W. Eliceiri, NIH Image to ImageJ: 25 years of image analysis, Nat. Methods **9**, 671 (2012).

[53] E. Meijering, O. Dzyubachyk, and I. Smal, Methods for cell and particle tracking, Method. Enzymol. **504**, 183 (2012).

[54] C. W. Extrand and S. I. Moon, Indirect methods to measure wetting and contact angles on spherical convex and concave surfaces, Langmuir **28**, 7775 (2012).

[55] D. Vella and P. D. Metcalfe, Surface tension dominated impact, Phys. Fluids **19**, 072108 (2007).

[56] S. Gaudet, G. H. McKinley, and H. A. Stone, Extensional deformation of Newtonian liquid bridges, Phys. Fluids **8**, 2568 (1996).